Orig Life Evol Biosph (2017) 47:123–143
DOI 10.1007/s11084-016-9516-z

PREBIOTIC CHEMISTRY

Glycine Polymerization on Oxide Minerals

Norio Kitadai[1] · **Hiroyuki Oonishi**[2] · **Koichiro Umemoto**[1] · **Tomohiro Usui**[1] · **Keisuke Fukushi**[2] · **Satoru Nakashima**[3]

Received: 18 May 2016 / Accepted: 14 July 2016 /
Published online: 29 July 2016

Abstract It has long been suggested that mineral surfaces played an important role in peptide bond formation on the primitive Earth. However, it remains unclear which mineral species was key to the prebiotic processes. This is because great discrepancies exist among the reported catalytic efficiencies of minerals for amino acid polymerizations, owing to mutually different experimental conditions. This study examined polymerization of glycine (Gly) on nine oxide minerals (amorphous silica, quartz, α-alumina and γ-alumina, anatase, rutile, hematite, magnetite, and forsterite) using identical preparation, heating, and analytical procedures. Results showed that a rutile surface is the most effective site for Gly polymerization in terms of both amounts and lengths of Gly polymers synthesized. The catalytic efficiency decreased as rutile > anatase > γ-alumina > forsterite > α- alumina > magnetite > hematite > quartz > amorphous silica. Based on reported molecular-level information for adsorption of Gly on these minerals, polymerization activation was inferred to have arisen from deprotonation of the NH_3^+ group of adsorbed Gly to the nucleophilic NH_2 group, and from withdrawal of electron density from the carboxyl carbon to the surface metal ions. The orientation of adsorbed Gly on minerals is also a factor influencing the Gly reactivity. The examination of Gly-mineral interactions under identical experimental conditions has enabled the direct

✉ Norio Kitadai
nkitadai@elsi.jp

[1] Earth-Life Science Institute, Tokyo Institute of Technology, 2-12-1, Ookayama, Meguro-ku, Tokyo 152-8550, Japan

[2] Institute of Nature and Environmental Technology, Kanazawa University, Kakuma, Kanazawa, Ishikawa 920-1192, Japan

[3] Department of Earth and Space Science, Graduate School of Science, Osaka University, 1–1 Machikaneyama, Toyonaka, Osaka 560-0043, Japan

comparison of various minerals' catalytic efficiencies and has made discussion of polymerization mechanisms and their relative influences possible Further systematic investigations using the approach reported herein (which are expected to be fruitful) combined with future microscopic surface analyses will elucidate the role of minerals in the process of abiotic peptide bond formation.

Keywords Amino acid · Astrobiology · Chemical evolution · Peptide · Protein

Introduction

It has long been suggested that mineral surfaces played a key role in amino acid polymerization processes, a necessary step for the chemical evolution of life on the primitive Earth (Rode 1999; Lambert 2008). As many as 1000 mineral species were already present on Earth at the time of life's origin 4.5–4.0 billion years ago (Cleaves et al. 2012). Given the ubiquity of mineral–water interfaces on the Earth's surface, it is almost impossible to envision prebiotic chemistry scenarios leading to the origin of life without interfacial processes. To date, numerous experiments have been conducted to evaluate amino acid polymerization reactivity on a wide variety of oxide minerals and clays. Results have demonstrated their positive influences with regard to reaction rate, peptide length, and the amount of polymers synthesized. For example, Table 1 presents experimentally obtained results for amino acid polymerization on oxide minerals reported since 1990. Nevertheless, it remains unclear which mineral species played the key role for abiotic peptide formation because results from different laboratories mutually contrast one another, and to a great degree in many cases. For instance, Shanker et al. (2012) conducted a heating experiment of glycine (Gly) on TiO_2 at 120 °C for 1–35 days after drying the Gly–TiO_2 mixture at 90 °C for 3 h. They observed dimerization of Gly to glycylglycine (GlyGly) and diketopiperazine (DKP) with yields higher than 10 %. In contrast, no appreciable signal for Gly polymerization was detected on the anatase surface by a thermogravimetric analysis of the 100–200 °C range with a heating rate of 5 °C min^{-1} (Lambert 2009, Lambert et al. 2013). Using amorphous silica as a mineral catalyst, Georgelin et al. (2013) observed nearly complete conversion of Gly to DKP by heating for a few minutes at 160 °C in the dry state. Upon adsorption from the gas phase, however, only linear peptides up to 11-mer were formed from Gly on a SiO_2 pellet (Martra et al. 2014). As another example, dry heating of Gly on alumina at 85 °C for 7 days produced GlyGly as a major product (13.06 %) with minor amounts of DKP (1.94 %) and triglycine (Gly_3, 1.02 %) (Bujdak and Rode 2003). A similar experiment with prolonged heating time (for 28 days) caused dominant production of DKP (16.1 %) with lower yields of GlyGly (5.6 %), Gly_3 (1.9 %), and Gly_4 (0.8 %) (Bujdak and Rode 2003).

These discrepancies clearly indicate that the catalytic activities of minerals for amino acid polymerization heavily depend on experimental conditions such as heating temperature, duration time, preparation procedure of mineral–amino acid mixtures, and their mixing ratio. One approach to resolve the complexity is to address a specific mineral–amino acid combination and to examine their interaction with systematically differing reaction conditions in particular (e.g., Meng et al. 2004; Ben Shir et al. 2012; Lambert et al. 2013). By combining advanced surface analytical

Table 1 Summary of experimentally obtained results reported for amino acid polymerization on oxide minerals

Amino acids	Minerals	Mixing ratio (AA / M)	Reaction conditions	Peptides	Ref.
Gly, Ala, Ile, Leu, Met, Phe, Val	silica, alumina	50 mg / 500 mg	chemical vapor deposition at ~200 °C under vacuum	from Gly on silica: $Gly_{1–3}$, $cyc(Gly)_2$ from Gly on alumina: $Gly_{1–4}$, $cyc(Gly)_2$	a
Gly, Val	silica		chemical vapor deposition at 200 °C under vacuum	from Val: $Val_{2–6}$, $cyc(Val)_2$	b
Gly, Ala, Val, Leu, Pro, Tyr, Phe, Met, Thr, Trp	silica	0.5–2.0 g / 5 g	chemical vapor deposition at 170–240 °C under vacuum	$cyc(Gly)_2$ (13), $cyc(Ala)_2$ (55), $cyc(Val)_2$ (58), $cyc(Leu)_2$ (64), $cyc(Pro)_2$ (77)	c
Ala, Val, Leu	silica	4 g / 10 g	chemical vapor deposition at 220–240 °C under vacuum	$cyc(Ala)_2$ (44 %), $cyc(Val)_2$ (89 %), $cyc(Leu)_2$ (39 %)	d
Gly	silica, alumina	1 mL, 10 mM / 0.01 g	80 °C for 1–7 d with periodic addition of 1 mL water	on silica: Gly_2 (≤0.20), $cyc(Gly)_2$ (≤0.21) on alumina: Gly_2 (≤0.36), $cyc(Gly)_2$ (≤0.39)	e
Gly, Ala	silica, alumina	1 mL, 10 mM (or 0.1 mL, 100 mM) / 0.01 g	80 °C for 1–14 d with and without periodic addition of 1 mL (or 0.1 mL) water	from Ala on silica: Ala_2 (≤0.18), $cyc(Ala)_2$ (≤0.76) from Ala on alumina: Ala_2 (≤3.80), $cyc(Ala)_2$ (≤2.44)	f
Gly, Ala, Leu, Pro, Val	silica, alumina	0.1 mL, 100 mM / 0.01 g	80 °C for 7 d	from Gly: Gly_2 (0.12 % on silica, 13.06 % on alumina), $cyc(Gly)_2$ (0.32 % on silica, 1.94 % on alumina), Gly_3 (1.02 % on alumina) from Ala: Ala_2 (0.11 % on silica, 1.59 % on alumina), $cyc(Ala)_2$ (0.80 % on silica, 0.17 % on alumina) from Leu: Leu_2 (0.19 % on silica, 1.05 % on alumina) from Pro: Pro_2 (0.60 % on alumina) from Val: Val_2 (0.06 % on silica, 0.05 % on alumina), $cyc(Val)_2$ (0.18 % on alumina)	g
Gly	am. silica	0.066–2.7 × 10^{-4} mol / 1 g	heated under reflux in toluene	Gly_2 (≤92.4), $cyc(Gly)_2$ (≤44.3)	h
Ala	alumina (α-corundum, neutral, acidic, weakly acidic, and basic)	1 mmol / 1 g	95 °C for 1–14 d after drying at 80 °C for 3 h	on α-corundum: Ala_2 (≤0.4) on neutral: Ala_2 (≤3), $cyc(Ala)_2$ (≤0.5) on acidic: Ala_2 (≤1.3), $cyc(Ala)_2$ (≤0.15)	i

Table 1 (continued)

Amino acids	Minerals	Mixing ratio (AA / M)	Reaction conditions	Peptides	Ref.
				on weakly acidic: Ala_2 (≤3.2), $cyc(Ala)_2$ (≤0.5) on basic: Ala_2 (≤2.2), $cyc(Ala)_2$ (0.35)	
Ala	alumina (acidic, neutral, basic: all 155 m^2/g)	0.5 mL, 44 mg/mL / 0.5 g	55, 80, 100, or 120 °C up to 400 h after drying at RT for 1 d	on acidic: Ala_2 (≤1.7), $cyc(Ala)_2$ (≤0.3), Ala_3 (≤0.2) on neutral: Ala_2 (≤2.5), $cyc(Ala)_2$ (≤1.1), Ala_3 (≤0.6) on basic: Ala_2 (≤3.5), $cyc(Ala)_2$ (≤1), Ala_3 (≤0.8)	j
Gly, Ala, Leu, Pro, Val	neutral pH activated alumina	1 mmol / 1 g	85 °C for 1–28 d after drying at 85 °C for 3 h	from Gly: Gly_2 (≤16), $cyc(Gly)_2$ (≤6), Gly_3 (≤2), Gly_4 (≤1) from Ala: Ala_2 (≤7.5), $cyc(Ala)_2$ (≤6) from Leu: Leu_2 (≤5) from Val: Val_2 (≤2)	k
Gly, Ala, Leu, Pro, Val	γ-alumina	1 mmol / 1 g	85 °C for 28 d after drying at 85 °C for 3 h	from Gly: Gly_2 (5.6), $cyc(Gly)_2$ (16.1), Gly_3 (1.9), Gly_4 (0.8) from Ala: Ala_2 (7.5), $cyc(Ala)_2$ (7.5) from Leu: Leu_2 (4.7) from Val: Val_2 (2.0)	l
Gly	am. silica (380 m_2/g)	50 mL, 0.01–0.50 M / 1.5 g	heating rate of 5 °C/min in dry gas flow after a selective adsorption procedure[##]	DKP formed at temperatures from 155 to 195 °C	m
Gly, Ala	ferrihydrite (~200 m^2/g)	Wet exp.: 2 mL, 100 mM / 200 mg Dry exp.: 0.5 mL, 100 mM / 50 mg	Wet exp.: 95 °C for 24 h or 1w in a closed vial Dry exp.: 95 °C for 24 h or 1w after drying at RT	Wet exp.: Gly_2 (≤0.035), Gly_3 (<0.001), Ala_2; (≤0.0044), Ala_3 (<0.001) Dry exp.: Gly_2 (≤0.096), Gly_3 (<0.004), Ala_2 (≤0.091), Ala_3 (<0.004)	n
Gly, Ala, Lys	am. silica (380 m_2/g)	50 mL, 0.03–0.50 M / 1.5 g	heating rate of 5 °C/min in dry gas flow after a selective adsorption procedure[##]	amide bonds formed around 150–170 °C	o
Gly, Ala, Glu, Leu, Lys	am. silica (380 m_2/g), anatase		heating rate of 5 °C/min in dry gas flow after a selective adsorption procedure[##]	on am. silica: cyclic dimers of each amino acid formed at 150–160 °C on anatase: no peptide formation was observed	p
Gly, Ala, Glu, Asp	hydroxyapatite	2 mL, 1 M / 400 mg	110–190 °C for 10 h in air	Gly_2, Ala_2 (≤0.28), $cyc(Ala)_2$, Glu_2 (≤0.06), Asp_2 (≤0.1)	q

Table 1 (continued)

Amino acids	Minerals	Mixing ratio (AA / M)	Reaction conditions	Peptides	Ref.
Gly, Glu	aluminum oxide	0.02 mol Gly + 0.01 mol Gln / 0.100 g	175–190 °C for 20 min	Gly-Glu-$(Gly\text{-}Glu)_n$ polymer	r
Gly, Ala	α-FeOOH (57.4 m^2/g), β-FeOOH (30.37 m^2/g), α-Fe_2O_3 (7 m^2/g), ZnO, TiO_2	0.1 mL, 0.01 M / 0.1 g	50, 90, or 120 °C for 1–35 d after drying at 90 °C for 3 h	on α-FeOOH: DKP (≤30.7), Gly_2 (≤23.2), Gly_3 (≤11.7), $cyc(Ala)_2$ (≤13.5), Ala_2 (≤10.6) on β-FeOOH: DKP (≤10.1), Gly_2 (≤10.2), Gly_3 (trace), $cyc(Ala)_2$ (≤5.9), Ala_2 (≤5.69) on α-Fe_2O_3: DKP (≤85.2), Gly_2 (≤0.69), Gly_3 (trace), $Cyc(Ala)_2$ (≤50.3), Ala_2 (≤0.4) on ZnO: DKP (≤9.21), Gly_2 (≤6.34), Gly_3 (trace), $cyc(Ala)_2$ (≤4.32), Ala_2 (≤3.21) on TiO_2: DKP (≤20.2), Gly_2 (≤11.8), Gly_3 (trace), $cyc(Ala)_2$ (≤6.95), Ala_2 (≤4.98)	s
Gly, Gln	rutile (130–190 m^2/g), anatase (200–220 m^2/g)	0.02 mol Gly + 0.01 mol Gln / 0.1 g	175–190 °C for 1 h with and without room light	Polypeptide of ~4 (Gly-Gln) units (6 % on rutile, 23 % on anatase)	t
Ala, Arg	anatase (70 m^2/g)			AlaArg (major), ArgAla (minor)	u
Gly	am. silica (380 m_2/g)	0.03 M / 30 g/L	heating rate of 5 °C/min under dry air flow after a selective adsorption procedure[##]	DKP (~100 % after heating up to 160 °C)	v
Gly	am. silica (380 m_2/g), γ-alumina, anatase (165 m_2/g)		heating rate of 5 °C/min under dry air flow after a selective adsorption procedure[##]	on am. silica: DKP formed at 165 °C on γ-alumina: DKP formed at 150 °C on anatase: no peptide formation was observed	w
Gly	SiO_2, TiO_2		chemical vapor deposition at 433 K under vacuum	on SiO_2: $Gly_{3–11}$ on TiO_2: $Gly_{2–16}$, DKP	x

a, Basiuk et al. 1990–1991; b, Gromovoy et al. 1991; c, Basiuk et al. 1991; d, Basiuk 1992; e, Bujdak and Rode 1997a; f, Bujdak and Rode 1997b; g, Bujdak and Rode 1999; h, Ogawa et al. 1999; i, Bujdak and Rode 2001; j, Basiuk and Sainz-Rojas 2001; k, Bujdak and Rode 2002; l, Bujdak and Rode 2003; m, Meng et al. 2004; n, Matrajt and Blanot 2004; o, Stievano et al. 2007; p, Lambert 2009; q, Wu et al. 2011; r, Leyton et al. 2011; s, Shanker et al. 2012; t, Leyton et al. 2012; u, Jaber et al. 2013; v, Georgelin et al. 2013; w, Lambert et al. 2013; x, Martra et al. 2014. [##] for selective adsorption procedure, see Meng et al. (2004)

techniques, some information has been obtained for interfacial phenomena that engender the activation of amino acids. However, because of the difficulty in characterizing physical and chemical properties of adsorbed amino acids at the molecular level, the mechanisms controlling the surface reactivity of amino acids remain unclear.

Another possible approach is to examine amino acid polymerization on various minerals under identical experimental conditions. Results enable direct comparison of the catalytic activity of each mineral. Therefore, favorable mineral–amino acid combinations can be ascertained. The variations are a useful foundation for deducing the surface mechanisms of amino acid polymerization on minerals if good and poor mineral catalysts possess different surface properties. This approach provides characteristic information that is unobtainable when examining single mineral–amino acid combinations, as introduced above. Such mutually independent information is expected to be useful: when combined with future microscopic surface analyses, it can be applied to gain a thorough understanding of the roles of minerals in abiotic peptide bond formation. Additionally, if an experiment is conducted under conditions that are relevant to a geochemical situation on the primitive Earth, results can be applied directly to discuss plausible environments supporting the chemical evolution of amino acids with regard to the distribution and abundance of mineral species.

For this study, we examined the polymerization of Gly on nine oxide minerals: amorphous silica, quartz, α-alumina and γ-alumina, hematite, magnetite, anatase, rutile, and forsterite. Gly was chosen because it is the simplest amino acid. Gly has been synthesized in many experiments simulating primitive Earth environments and interstellar medium conditions (Zaia et al. 2008). In fact, it has frequently been observed in carbonaceous chondrites in the highest concentration among detected protein amino acids (Glavin et al. 2011). Because of its simple structure, Gly has been used in many polymerization experiments (Table 1). The nine oxide minerals examined in the present study do not necessarily represent major mineral constituents of the upper crust of the primitive Earth (Schoonen et al. 2004; Hazen et al. 2008; Cleaves et al. 2012). Rather, they were selected because detailed surface analyses have been made for interaction with simple organic molecules, especially for silica (Rimola et al. 2013), alumina (Kelber 2007), and titanium oxides (Thomas and Syres 2012). Together with the polymerization behaviors of Gly observed in this study, this information is useful for assessing the Gly–surface interaction that enhances Gly polymerization. It is noted that microscopic analyses of the adsorption behavior of Gly have typically been conducted using a polished mineral plate as the adsorbent. In contrast, this study used fine mineral powders with large specific surface areas (Table 2) in order to obtain sufficient yields of Gly polymers for identification and quantification. The mineral powders would have various types of crystal face and surface defects/vacancies with mutually different degrees. However, it has been shown that the Gly–surface interactions on different crystal faces of rutile are similar to each other (Lerotholi et al. 2009 for the (110) surface; Wilson et al. 2011 for the (011) surface). A scanning tunneling microscopic study of Gly on TiO_2(110) surface has observed no discernible effect of surface defects on the structure of adsorbed Gly (Qiu and Barteau 2006). These observations indicate that the surface structure of a mineral is not a primary factor controlling Gly adsorption, hence it should not be one for Gly polymerization either. In fact, as will be shown in the discussion section, the mineral-catalyzed Gly polymerization observed in this study could be reasonably explained based on the reported surface analytical results for the corresponding Gly–mineral systems without consideration of the difference in surface characteristics.

To facilitate data interpretation, our experiment was conducted at 80 °C in dry conditions without temperature or water content fluctuations. Simple and mild conditions are likely to have prevailed in terrestrial environments on the primitive Earth, such as tidal pools and dry

lagoons, where the purification and concentration of abiotically formed amino acids might be realized through natural processes (Kitadai et al. 2011; Stueken et al. 2013).

Experimental

Gly (99.9 % purity) was purchased from Peptide Institute Inc., and was used without further purification. Forsterite powder was provided by Marusu Glaze Co. Ltd., whereas the other minerals (Table 2) were purchased from Kojundo Chemical Lab. Co. Ltd. X-ray diffraction analysis showed that all minerals are structurally pure except for rutile, which includes a small amount of anatase as an impurity (Fig. A1). The specific surface areas of the minerals were measured using the single-point N_2-BET method with a surface area analyzer (Flowsorb III 2305; Shimadzu Corp.). The values and other physical properties of the minerals are presented in Table 2.

Gly–mineral mixtures were prepared by immersing mineral powders in a 4 mL of 3.575 mM Gly solution in a 10-mL PTFE vessel, and by stirring for 3 h at room temperature, after which the suspensions were dried in the air at 50 °C for 24 h. The amount of mineral sample added to each PTFE bottle was adjusted to obtain the Gly–mineral mixing ratio of 10 Gly molecules per 1 nm^2 of surface area. For example, 100 mg of forsterite was mixed with 4 mL of 3.575 mM Gly solution. Assuming a molecular cross-section of approximately 0.2 nm^2 for Gly (Jonsson and Kvick 1972), and assuming uniform adsorption, approx. 50 % of Gly molecules were inferred to have attached directly to the mineral surface, with the remainder forming di-layer adsorption. The PTFE vessels were then closed using a PTFE lid. They were shielded in a screw-capped stainless steel outer vessel. To accelerate interactions between Gly and the minerals, the vessels were heated in an electric oven at 80 °C for 1–10 days. Control experiments were also conducted in the absence of a mineral.

After heating, each product was dissolved in distilled and deionized water (8 mL), was centrifuged for 10 min at 3000 rpm, and was filtrated through a 0.20-μm pore size filter. Control experiments demonstrated that this procedure can release all adsorbed Gly and Gly polymers from all oxide minerals to water (adsorbed amounts were checked using the

Table 2 Properties of the oxide minerals used for this study

Mineral	Formula	Purity (%)[a]	Particle diameter (μm)[a]	BET surface area ($m^2\ g^{-1}$)	pH[b]
Amorphous silica	SiO_2	>99.9	1	3.67	5.1
Quartz	SiO_2	99.9	0.8	12.7	5.7
α-alumina	Al_2O_3	>99.99	1	4.97	6.4
γ-alumina	Al_2O_3	99.9	2–3	95.7	7.0
Hematite	Fe_2O_3	99.9	1	3.75	6.0
Magnetite	Fe_3O_4	99	<1	5.14	7.3
Anatase	TiO_2	99	<1	6.87	6.8
Rutile	TiO_2	99.99	2	2.37	4.5
Forsterite	Mg_2SiO_4	–	1.2	8.61	9.0

[a] all values were provided from manufacturers except for the particle diameter of anatase, which was measured in this study by using a laser diffraction grain size analyzer (SALD-2200, SHIMADZU)

[b] measured after mixing with 4 mL of Gly solution with the Gly–mineral mixing ratio of 10 Gly molecules per 1 nm^2 of surface area (see experimental section)

following HPLC measurements). Gly and Gly peptides (GlyGly, Gly_3, Gly_4 and Gly_5) were analyzed according to the procedure described by Kitadai et al. (2011) using an HPLC system (Jasco Corp.) equipped with post-column derivatization with *o*-phthalaldehyde and a fluorescence detector (345 nm for excitation and 455 nm for emission). Peak separation in the chromatograms was achieved using a cation-exchange column (AApak Na II-S2; Jasco Corp.) with five citrate buffer solutions having different citrate concentrations and pH values. A typical chromatogram was shown in an earlier report (Kitadai et al. 2011). DKP was analyzed using another HPLC system (8020 series; Tosoh Corp.) equipped with a UV detector operated at 200 nm wavelength. The eluent was 10 mM sodium hexane sulfonate adjusted to pH 2.5 by adding phosphoric acid. A reverse-phase column (Hydrosphere C18; YMC Co. Ltd.) was used at 37 °C. For each HPLC analysis, the measurement error in concentration was less than 2 %, as estimated by measuring a standard sample solution three times.

To observe the surface morphology and Gly distribution on minerals, scanning electron microscopy was conducted for the Gly–mineral mixtures prepared via the immersing, stirring, and drying procedures described above. The dry mixtures were deposited on a gold plate, and were examined using a scanning electron microscope (SEM, S-3400 N; HITACHI) with an energy dispersive X-ray detector (EDX, XFlash 5010; Brucker). All the X-ray maps (1024 × 768) were obtained with an incident beam energy of 15 keV and the magnification of ×4000.

Unless otherwise noted, all experiments were conducted at around 25 °C, with the temperature controlled using an air-conditioner.

Results

Figure 1 shows SEM images (a–h) and C distributions (j–q) of the nine oxide minerals measured after mixing with Gly (see experimental section). The C signal showed similar contrast patterns to the mineral distributions, indicating that Gly is present homogeneously on the mineral surfaces. It is noteworthy that an N Kα emission occurs at 0.392 keV, which is close to that of O (0.525 keV). Therefore, because oxide minerals exhibit an intense O band, no clear N signal was observed in the EDX spectra of all samples. It is also noted that Au, the material of the sample plate, shows a minor Lγ2 emission at 0.258 keV. Due to its proximity to the C Kα signal (0.277 keV), Au has an influence on the mapping results of C. In the absence of Gly, for example, the apparent C distribution patterns correlate well with Au, rather than minerals (Fig. A2). In contrast, the clear correlations between C and mineral outlines seen in Fig. 1 indicate that the influence of Au is small in the examined Gly/mineral mixing ratio, and observed C patterns are attributable to Gly distribution.

Figure 2 presents yields, defined here as the percentage of Gly incorporated into each polymer, of Gly polymers synthesized on each mineral as a function of the heating time. In many cases, GlyGly was formed initially as a dominant polymerization product. The fraction decreased with time in accordance with the increases of the fractions of other Gly polymers. Exceptions for this trend were observed on α-alumina (Fig. 2a), forsterite (Fig. 2d), and γ-alumina (Fig. 2e), where the yield of GlyGly continued increasing during the heating time. Another major product of Gly polymerization is DKP. On amorphous silica (Fig. 2b), hematite (Fig. 2f), magnetite (Fig. 2g), and quartz (Fig. 2h), the DKP yield increased with time and came to show comparable or higher values than that of GlyGly at the later stage of the heating experiment. Larger Gly polymers were also observed on anatase (Fig. 2c), γ-alumina (Fig. 2e), and rutile (Fig. 2i). On rutile (Fig. 2i), up to 5-mer was formed with relative abundances of

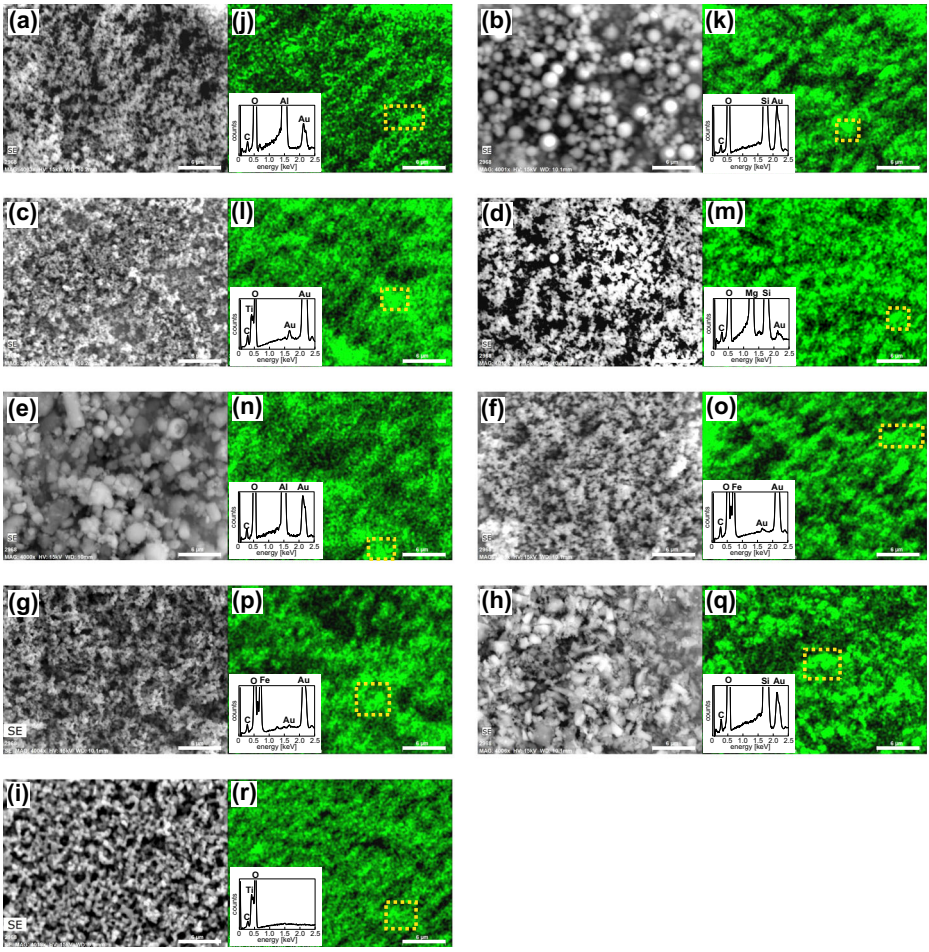

Fig. 1 SEM images and C distributions of **a**, **j** α-alumina, **b**, **k** amorphous silica, **c**, **l** anatase, **d**, **m** forsterite, **e**, **n** γ-alumina, **f**, **o** hematite, **g**, **p** magnetite, **h**, **q** quartz, and **i**, **r** rutile measured after drying the corresponding Gly–mineral suspensions at 50 °C. Insert in (**j**–**r**) respectively shows EDX spectrum obtained at the area marked by yellow dots in each figure. White horizontal bars represent the length of 6 μm

Gly_3 > Gly_4 > Gly_5. Rutile had the strongest influence in promoting Gly polymerization in terms of the amount and the length of synthesized peptides. As a result of 10-days' heating, about 25 % of Gly was polymerized on rutile. The percentage decreased in the order of rutile > anatase > γ-alumina > forsterite > α-alumina > magnetite > hematite > quartz > amorphous silica (Fig. 3). Amorphous silica exhibited the weakest promotion effect, but the total yield of Gly polymers on amorphous silica remained much higher than that observed without a mineral. Results show that only GlyGly was formed with a yield up to approximately 0.01 %.

Discussion

Why did the oxide minerals promote Gly polymerization? What caused the observed differences of the amounts and lengths of Gly polymers synthesized on the minerals? In this section

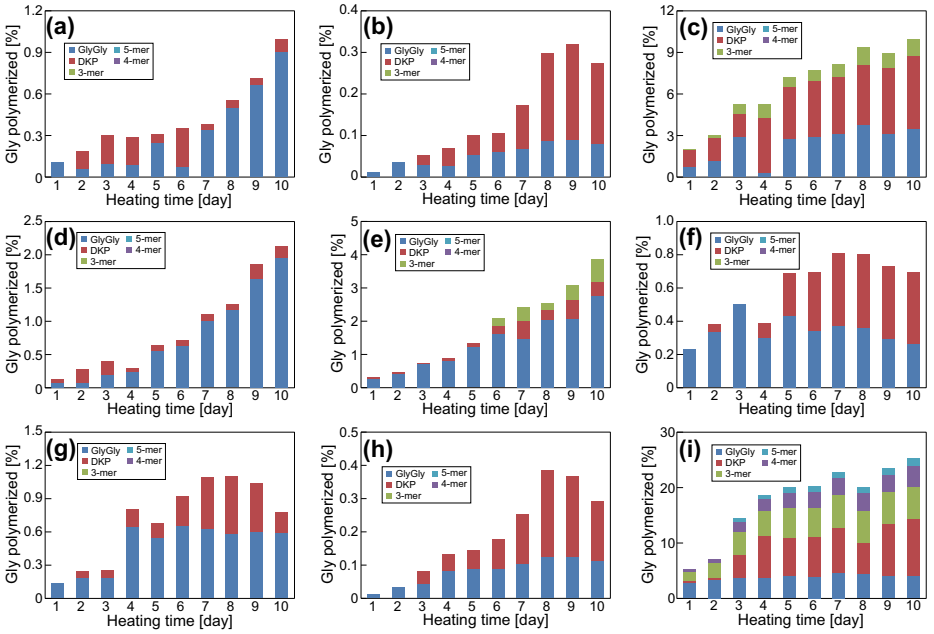

Fig. 2 Yields of Gly polymers synthesized on **a** α-alumina, **b** amorphous silica, **c** anatase, **d** forsterite, **e** γ-alumina, **f** hematite, **g** magnetite, **h** quartz, and **i** rutile at 80 °C as a function of heating time (the yield is defined as percentage of Gly incorporated into each polymer). The vertical scale differs for each figure

we discuss these two questions based on the physical and chemical properties of Gly and Gly polymers on the minerals reported in the literature.

From a thermodynamic point of view, the monomer–polymer equilibria shift toward the polymer side if Gly polymers interact with minerals that have higher adsorption energies than Gly monomer does. This effect can be evaluated quantitatively for amorphous silica using reported adsorption Gibbs energies $\left(\Delta_r G^o_{ad.}\right)$ of Gly and Gly peptides on this mineral (Basiuk and Gromovoy 1994; Basiuk et al. 1995). Results show that the $\Delta_r G^o_{ad.}$ of Gly peptides in water were lower than that of Gly. Therefore, adsorption might indeed favor polymerization. However, the decreases of $\Delta_r G^o_{ad.}$ as a function of chain length were small (approx. 0.2 kJ residue^{-1}) compared with the Gibbs energy necessary for the synthesis of a mole of peptide bond

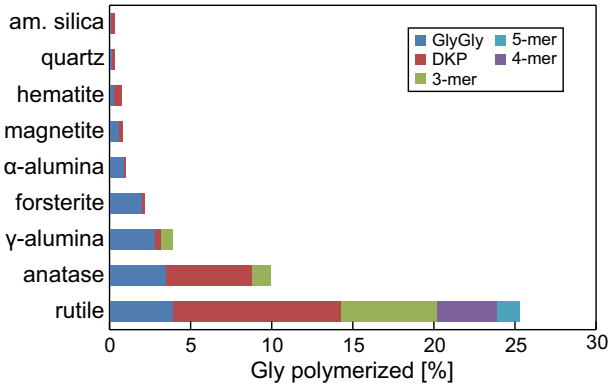

Fig. 3 Yields of Gly polymers synthesized on nine oxide minerals after 10 days' heating at 80 °C

(17.1 kJ mol^{-1}; Kitadai 2014). Consequently, the thermodynamic drive of adsorption for peptide bond formation is limited. Similar calculations cannot be conducted for other oxide minerals because experimental $\Delta_r G^o_{ad.}$ values of Gly and Gly peptides are not available in the literature. However, the values of $\Delta_r G^o_{ad.}$ and the difference in the $\Delta_r G^o_{ad.}$ of Gly and Gly peptides on each mineral are expected to be small because no adsorption was observed in this study for any compound on any mineral in water. This factor is therefore regarded as making no substantial contribution to the observed active polymerizations of Gly on the minerals (Figs. 2 and 3).

Gly polymerization produces water molecules as well as Gly polymers (e.g., 2Gly → GlyGly + H_2O). Therefore, the reaction is expected to proceed favorably as the fugacity of water decreases. Figure 4 shows equilibrium water fugacities with polymerizations of Gly to GlyGly, DKP, and Gly_3 as functions of temperature. The calculation procedure used for these curves is shown in Appendix C together with the thermodynamic dataset that was used. At 80 °C, the equilibrium fugacities for the GlyGly, DKP, and Gly_3 formations are 0.029, 0.048, and 0.023 bar, respectively, which are close to the saturated water vapor pressure at room temperature (0.03 ± 0.01 at 25 ± 5 °C). If sample preparations are conducted at a vapor pressure below the equilibrium values, dehydration–polymerization of Gly can proceed at 80 °C until the vapor pressure reaches equilibrium. It is difficult to estimate precisely the thermodynamically attainable concentrations of Gly polymers because the vapor pressure was not controlled in this study (but it is typically 50 ± 20 %), and because uncertainties exist in the thermodynamic parameters used in the calculation (the error in $\Delta_r G^o$ of ±1 kJ mol^{-1} leads to variation of the equilibrium of vapor pressure by a factor of 1.5; see Eq. A1). Additionally, in the presence of minerals, mineral surfaces might adsorb some fraction of water vapor in the reaction vessel, thereby inducing further Gly polymerization. However, decreased vapor pressure does not markedly accelerate the reaction. Kitadai et al. (2011) examined its influence by heating Gly powder at 140 °C in a PTFE bottle with vapor pressure controlled by $MgSO_4$/$MgSO_4 \cdot H_2O$ equilibrium. The equilibrium vapor pressure with $MgSO_4$ hydration was 2×10^{-3} bar at 140 °C, which is much lower than those of Gly polymerization at the same temperature (0.8, 1.3, 0.7 bar for the GlyGly, DKP, and Gly_3 formations, respectively).

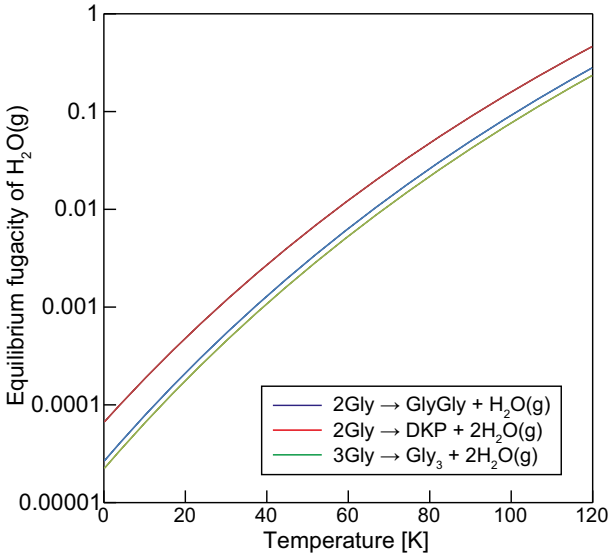

Fig. 4 Fugacity of water equilibrated with polymerization of Gly to GlyGly, DKP, and Gly_3 as a function of temperature

Nonetheless, the yields of Gly polymers after 20-days' heating were only around 0.4 %, with DKP being the major product. The total yield is less than those produced on oxide minerals (except for amorphous silica and quartz; Figs. 2b and h) in spite of the higher temperature and longer heating time. Consequently, although the vapor pressure is an important parameter to make Gly polymerization thermodynamically favorable, the value cannot explain the kinetic aspects of the observed polymerization behaviors of Gly on minerals.

Nevertheless, thermodynamic calculation (Fig. 4) is useful considering the mechanisms controlling the structure of Gly polymers (cyclic vs. linear) formed on oxide minerals. It is seen in Fig. 4 that DKP has higher equilibrium water fugacity than the GlyGly formation. Thus, if the water fugacity in the reaction vessel is lower than the Gly → GlyGly conversion, the condition is also thermodynamically favorable for DKP formation. The water fugacity in the reaction vessel is expected to increase along with the progress of Gly polymerization, and shift the reaction conditions toward a less thermodynamically favorable state. The increase of water fugacity might have a stronger influence on the formation of GlyGly than DKP owing to the lower equilibrium water fugacity (Fig. 4). It might be a reason why a major polymerization product on amorphous silica, hematite, magnetite, and quartz changed gradually from GlyGly to DKP with time (Fig. 2). It is also noteworthy that the speciation of Gly influences the thermodynamics of Gly polymerization (Kitadai 2014). The speciation change of Gly from the zwitterionic form (NH_3^+-CH_2-COO^-) to the combination of zwitterionic and anionic Gly (NH_2-CH_2-COO^-) favors the formation of linear Gly peptides over DKP. Given the alkaline pH of suspension (pH 9.0; Table 2) and the second dissociation constant of Gly (pK_2 = 9.78 at 25 °C; Kitadai 2014), Gly speciation on forsterite is expected to be partly anionic in addition to zwitterionic. The preferential formation of GlyGly over DKP on this mineral (Fig. 2d) might be caused by the pH effect. In contrast, the structures of polymers formed on the titanium and aluminum oxides (Figs. 2 and 3) are not explainable based on the thermodynamic calculation for pure Gly polymerization (Fig.4) and the suspension pH (Table 2). To understand the polymerization behaviors of Gly on these minerals, the surface–Gly interaction needs to be taken account in addition to the consideration of these factors.

The adsorption behavior of Gly on rutile, the most effective catalyst among the minerals used in this study (Fig. 3), has been examined using both experimental and computational investigations. Results have demonstrated that direct interaction with a rutile surface stabilizes Gly in the anionic state, whereas zwitterionic Gly dominates in the second and higher adsorption layers (Qiu and Barteau 2006; Lerotholi et al. 2009; Tonner 2010; Wilson et al. 2011; Monti et al. 2012). In the present study, the surface coverage of Gly on rutile corresponds to double-layer adsorption. Consequently, approx. 50 % of adsorbed Gly is expected to be present in the anionic state, whereas the other is in the zwitterionic state. The anionic–zwitterionic speciation pair is the most favorable combination for peptide bond formation. For Gly dimerization to GlyGly at 140 °C in an aqueous solution, for instance, the dimerization rate of $Gly^-/Gy^\pm$ pair is about 100 times faster than that of a $Gly^\pm/Gly^\pm$ pair (Sakata et al. 2010). The superiority arises from the fact that the nucleophilic amino group ($-NH_2$) of an anionic Gly can attack the deprotonated carboxyl group ($-COO^-$) of neighboring zwitterionic Gly without electrical repulsion between the two molecules. Although speciation dependences are not reported in the literature for the formation rates of longer Gly peptides, the co-existence of anionic and zwitterionic states would also favor their polymerizations because of the similar reaction mechanisms.

Another Gly–rutile interaction that might hasten Gly polymerization is changes in the electrostatic properties of the carboxyl group of adsorbed Gly on rutile. Actually, Gly is known to adsorb on rutile through the two carboxyl O atoms forming a bidentate coordination to two titanium ions (Tonner 2010; Wilson et al. 2011; Monti et al. 2012). The binding mode is

expected to withdraw electron density from the carboxyl carbon, making it sufficiently electrophilic to undergo nucleophilic attack by the nitrogen atom of the amino group of another Gly. It would also serve to weaken the electrical repulsion among negatively charged anionic Gly; so polymerization between Gly^- and Gly^- might also proceed with good efficiency.

Similar adsorption behaviors of Gly have been observed on γ-Al_2O_3, where the carboxyl O atoms of anionic Gly bind electrostatically to the surface Al^{3+} ions (Tzvetkov et al. 2004). One possible difference is that the binding energy between the carboxyl oxygens and surface metal ions (Ti or Al; quantitative comparison is impossible because no binding energy for a Gly/γ-Al_2O_3 system is available in the literature). A specific feature of rutile and anatase is the presence of 3d states of Ti^{4+}. Their 3d states are empty and split into lower t_{2g} and higher e_g states. Empty t_{2g} states are arranged toward the faces of octahedra of oxygens surrounding Ti^{4+} ions. They might be able to accept electrons from carboxyl oxygen easily. The Al ions in alumina have no such d state. Therefore, it might be possible that the binding energies of titanium oxides and alumina mutually differ because of the empty 3d states of Ti^{4+}. Another difference is the contribution of the amino group ($-NH_2$) to the surface binding of Gly on the minerals. On rutile, a computer calculation predicted that Gly forms hydrogen bonds between the amino group and the surface Ti ions (Tonner 2010). On γ-Al_2O_3, no experimental evidence has been obtained for the amino group-mediated interaction (Tzvetkov et al. 2004). Consequently, Gly on rutile is expected to orient the -NH_2 group toward the surface with anchoring of the -COO^- group (Tonner 2010), whereas Gly on γ-Al_2O_3 has a perpendicular orientation with the amino group pointing away from the surface (Tzvetkov et al. 2004). These differences in binding energy and surface orientation can influence the polymerization behavior of Gly, leading to the different yields and lengths of Gly polymers observed on these minerals (Fig. 3).

Anatase is the second most effective mineral catalyst for Gly polymerization, as shown in Fig. 3. Approximately 10 % of Gly was converted into GlyGly, DKP, and Gly_3 during 10-days' heating. A first-principles calculation predicted that Gly binds onto the surface in the form of neutral speciation (NH_2-CH_2-COOH). Anionic-state adsorption similar to that on rutile is slightly more unstable in energy than the neutral-state adsorption (Szieberth et al. 2010). It is noteworthy, however, that the calculations used for that study examined the adsorption behavior of a single Gly molecule on anatase surface. No lateral interaction among adsorbed Gly molecules was considered. The lateral interactions induce a strong H-bond cooperativity among adjacent Gly molecules, resulting in marked stabilization of charged Gly species over the neutral one (Rimola et al. 2013). In the surface coverage of Gly on the minerals applied in the present experiment, the binding structure of Gly on anatase can be reasonably regarded as similar to that on rutile. A difference in surface interaction that possibly caused the different polymerization behaviors of Gly on rutile and on anatase (Figs. 2 and 3) is the adsorption energy of Gly; 131 kJ mol^{-1} was calculated for the Gly–rutile system (Tonner 2010), whereas it was 107 kJ mol^{-1} for the Gly–anatase system (Szieberth et al. 2010).

A detailed spectroscopic analysis has been made for alanine (Ala) adsorption on α–alumina and γ-alumina using diffuse reflectance infrared spectroscopy (Garcia et al. 2007). Results show that adsorption on γ-alumina causes spectral shifts of Ala attributable to hydrogen bonds between the negatively charged carboxyl group of Ala ($-COO^-$) and the positively charged surface site (≡Al-OH_2^+). In contrast, no appreciable spectral modification was observed for Ala on α-alumina. Actually, thermodynamically, α-alumina is the most stable phase of alumina that crystallizes in the hexagonal system, whereas γ-alumina is a transitional alumina phase with a defective spinel-type structure (Garcia et al. 2007). Because of the defective structure, γ-alumina surface has Lewis acid and base sites (Al^{3+} and O^{2-} ions, respectively), thereby catalyzing a wide variety of chemical reactions (Garcia et al. 2007). The effects of α-alumina and γ-alumina on peptide bond formation

were previously evaluated by Bujdak and Rode (2001) by examining the dimerization of Ala on these minerals at 80 °C. As shown in our experimental results (Fig. 3), they observed Ala dimer on γ-alumina with higher yield than on α-alumina (3 % vs. 0.5 % after the 14-days' heating). It is noteworthy that the two alumina samples used in their experiment were not analyzed for specific surface area. Therefore, it is unclear whether the observed difference in catalytic activity arises from the difference of their surface area, or from specific surface interactions with Ala. Our experiment with a unified Gly–mineral mixing ratio (10 Gly molecules per 1 nm^2 of the surface) provided a clear demonstration that the surface structure of γ-alumina can accelerate peptide bond formation, and that its catalytic activity is higher than that of α-alumina. As is the case for titanium oxides (rutile and anatase), the different polymerization behaviors of Gly on α-alumina and γ-alumina (Figs. 2 and 3) are good examples exhibiting the importance of surface structure for the activation of amino acids.

The differences that arose from surface structure (rutile vs. anatase, α-alumina vs. γ-alumina) appear to be small compared with those from metal cations in oxide minerals (e.g., Ti vs. Al). Both titanium oxides showed higher catalytic efficiencies than that of α-alumina or γ-alumina; the two alumina surfaces synthesized greater amounts of Gly polymers than on hematite or magnetite, although even lower yields were observed on amorphous silica and quartz (Figs. 2 and 3). Why did the silica surfaces exhibit the lowest catalytic efficiency for the polymerization of Gly? Spectroscopic and computational investigations have shown that Gly adsorbs on silica in the form of a zwitterionic state (NH_3^+-CH_2-COO^-) through hydrogen bonds between the amino group and the surface silanol group (≡Si-O^- or ≡Si-OH) (Meng et al. 2004; Ben Shir et al. 2012). The carboxyl group makes a minor contribution to the binding, or none at all. In this adsorption configuration, no activation is expected for both the amino and carboxyl groups of Gly (i.e., deprotonation of the NH_3^+ group to the nucleophilic NH_2 group, and withdrawal of electron density from the carboxyl carbon). The very low yields of Gly polymers on silica (Fig. 3) are therefore consistent with the discussion presented above for the polymerization mechanism of Gly on TiO_2 and Al_2O_3. It is noteworthy that the formation of long Gly polymers (up to 11 units long) has been observed on silica when Gly adsorbed onto the surface from the gas phase (Martra et al. 2014). In gas-phase adsorption on silica, Gly binds on the surface in the form of a neutral state (NH_2-CH_2-COOH) through hydrogen bonds between the carboxyl group and the surface silanol group (≡Si-OH) (Lomenech et al. 2005; Costa et al. 2007; Lambert 2009). The adsorption mode is expected to be favorable for intermolecular interactions between the amino and carboxyl groups of neighboring Gly. Adsorption from the gas phase, however, is difficult to envision as a plausible geochemical phenomenon on the primitive Earth. Unless a reasonable scenario is given for abiotic formation of gas-phase amino acids, the contribution of silica to prebiotic peptide formation is expected to be small.

The other oxide minerals (hematite, magnetite, and forsterite) showed intermediate catalytic efficiencies for Gly polymerization among the examined minerals (Fig. 3). Unfortunately, molecular-level information in the literature about adsorption of Gly on these minerals is insufficient to discuss the surface mechanisms that catalyze Gly polymerization. The results shown in Fig. 3 might reflect electrostatic or structural properties of their surfaces if the Gly–surface interactions discussed above are also key factors activating the Gly polymerization on these minerals. We examined correlations between the total yield of Gly polymers on each mineral at a given heating time and various surface properties of the minerals such as the point of zero charge (pH_{ZPC}), the pH of Gly–mineral suspensions (Table 2), the interfacial dielectric constant, and the density of surface OH site (Pokrovsky and Schott 2000; Sverjensky 2005). No clear relation among these parameters has been obtained (data not shown). Regarding the electron orbit of metal ions,

Fe^{2+} or Fe^{3+} in hematite and magnetite has 3d states partially occupied by 5–6 d electrons. Smaller yields of Gly polymers on iron oxides than on titanium oxides suggest that electronic repulsion between 3d electrons of Fe ions and Gly might reduce the binding energy. This possibility cannot explain why the yield of Gly polymers on alumina is higher than that on iron oxides. Further study is needed, both for adsorption behaviors of Gly on minerals and for polymerization reactivity of the adsorbed Gly, to elucidate the underlying mechanisms controlling Gly–surface interactions that activate Gly polymerization. The results of such studies should enable the prediction of the most effective mineral species for prebiotic peptide bond formation on the primitive Earth.

Concluding Remarks

Dry heating experiments of Gly were conducted on nine oxide minerals (amorphous silica, quartz, α-alumina and γ-alumina, anatase, rutile, hematite, magnetite, and forsterite) at 80 °C for 1–10 days. The following conclusions were obtained:

1. Rutile showed the highest catalytic efficiency in both yield and length of Gly polymers synthesized. The efficiency decreased in the order of rutile > anatase > γ-alumina > forsterite > α-alumina > magnetite > hematite > quartz > amorphous silica (Fig. 3).
2. The active polymerization of Gly on rutile is inferred–based on reported molecular-level information for Gly adsorption on this mineral–to arise from deprotonation of the NH_3^+ group to the nucleophilic NH_2 group, and from withdrawal of electron density from the carboxyl carbon to the surface Ti ions (Fig. 5). Similar surface interactions are expected to occur on anatase and γ-alumina, with slight differences in binding energy and surface orientation of adsorbed Gly. In contrast, a silica surface interacts with the NH_3^+ group of zwitterionic Gly via hydrogen bonds, resulting in no activation of the functional groups of Gly, as was expected on the rutile surface. The interpretation is consistent with the very minor yields of Gly polymers found on quartz and amorphous silica (Fig. 3).
3. It remains unclear what electrostatic or structural properties of mineral surfaces control the Gly–surface interactions. Additional study is needed, both of adsorption behaviors of Gly on minerals and of polymerization reactivity of the adsorbed Gly, to elucidate the mechanisms underlying the interactions that activate Gly polymerization.

The surface mechanism of amino acid polymerization on minerals has long been discussed in experimental and theoretical works on this topic (Bujdak and Rode 1997a, b, Rode 1999,

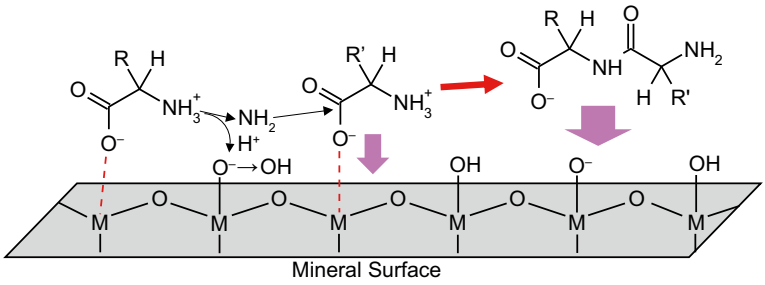

Fig. 5 Scheme showing the surface activation mechanisms of Gly polymerization on oxide mineral inferred from the results obtained in this study (Fig. 3)

2001; Lambert 2008; Deiana et al. 2013). Our conclusion for Gly–surface interactions that engender Gly polymerization (the 2nd one) is consistent with the idea explored in these discussions. It is noteworthy that evaluation of Gly-mineral interactions under identical experimental conditions made it possible to directly compare the catalytic efficiencies of various minerals, and to discuss polymerization mechanisms and their relative influences. Further systematic investigations of amino acid polymerization on minerals using the approach reported herein (which are expected to be fruitful) combined with future microscopic surface analyses will elucidate the role of minerals in the process of abiotic peptide bond formation.

Acknowledgments We thank Kunihiro Myojo for his help with SEM-EDX analysis of mineral samples. We also thank Lucy Kwok for her English correction of this manuscript. This manuscript was improved owing to valuable comments and suggestions from two anonymous reviewers. This research was financially supported by JSPS KAKENHI Grant Numbers 26800276 (Grant-in-Aid for Young Scientists (B)), 16H04074 (Grant-in-Aid for Scientific Research (B)), 16 K13906 (Grant-in-Aid for Challenging Exploratory Research), and 26106001 (Grant-in-Aid for Scientific Research on Innovative Areas).

Appendix 1

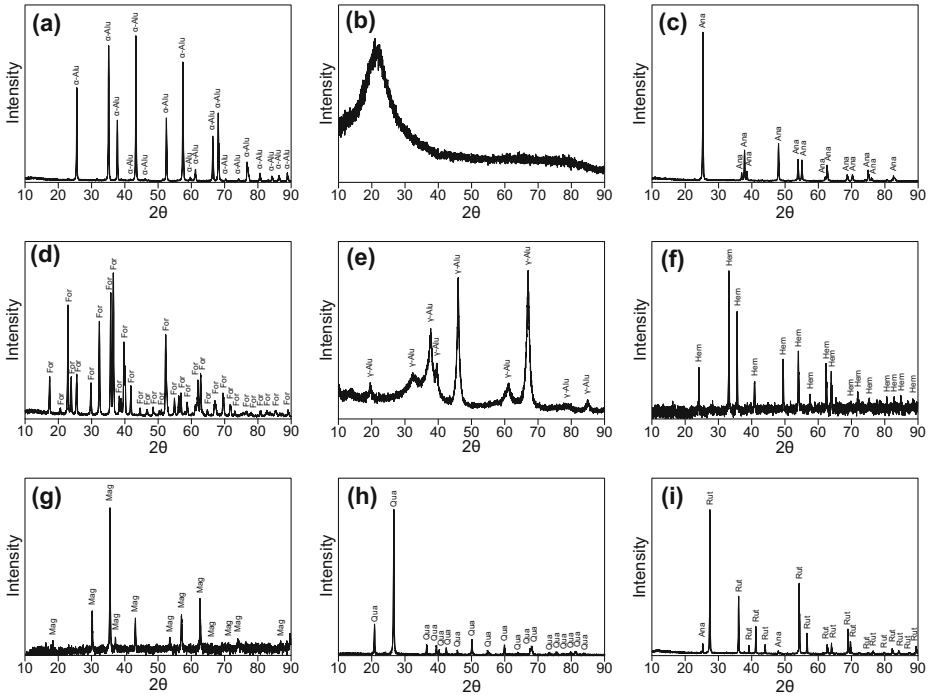

Fig. 6 XRD patterns of **a** α-alumina, **b** amorphous silica, **c** anatase, **d** forsterite, **e** γ-alumina, **f** hematite, **g** magnetite, **h** quartz, and **i** rutile measured using a Rigaku MiniFlex 600 with Cu Kα radiation. All runs were conducted with 2θ ranging from 10° to 90° using 0.02° 2θ step with a scan rate of 5° min^{-1}. Peak identifications were conducted on the basis of the PDF (Powder Diffraction File) published by International Centre for Diffraction Data. Abbreviation: α-Alu; α-alumina, Ana; anatase, For; forsterite, γ-Alu; γ-alumina, Hem; hematite, Mag; magnetite, Qua; quartz, Rut; rutile

Appendix 2

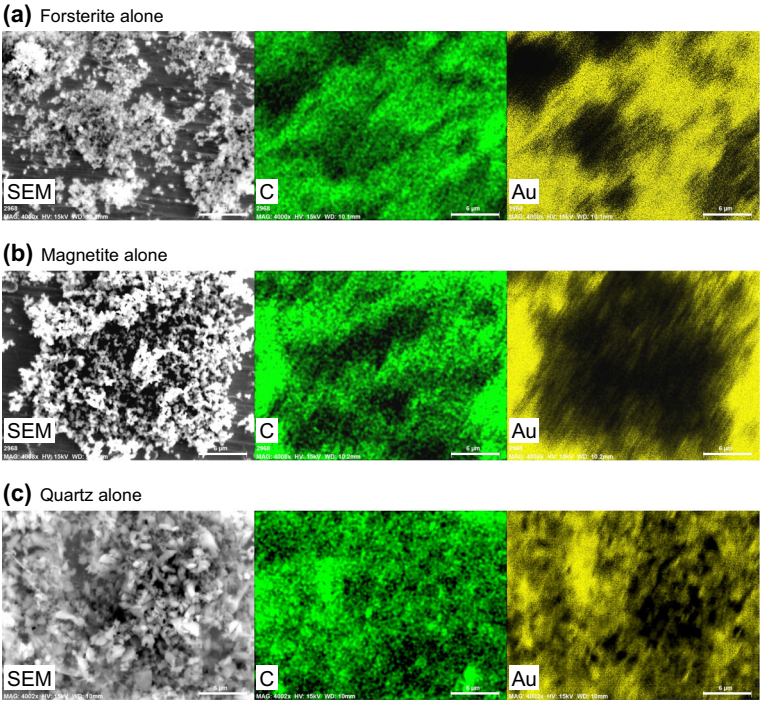

Fig. 7 SEM images and C and Au distributions of **a** forsterite, **b** quartz, and **c** magnetite measured without mixing with Gly. White horizontal bars represent the length of 6 μm

Appendix 3

The equilibrium fugacity of water with polymerization of Gly to GlyGly, DKP, and Gly_3 (Fig. 4) was calculated using the following equation

$$f_{H_2O} = \exp\left(\frac{-\Delta_r G^o}{\nu RT}\right) \tag{A1}$$

Therein, f_{H_2O} stands for the fugacity of H_2O(g), ν is the stoichiometric reaction coefficient of H_2O(g) in the reaction (one for GlyGly formation, two for DKP and Gly_3 formations), T represents the temperature in Kelvin, R denotes the gas constant (8.31447 J mol^{-1} K^{-1}), and $\Delta_r G^o$ denotes the standard Gibbs energy of reaction. The value of $\Delta_r G^o$ was calculated combining the standard molal Gibbs energy of formation (ΔGo) of the individual compounds involved in the reaction.

$$\Delta rGo = \sum \Delta G^o_{\text{products}} - \sum \Delta G^o_{\text{reactants}} \tag{A2}$$

The ΔG^o of all components at any temperature (T) and pressure (P) was calculated as the following.

$$G^o_{P,T} = G^o_{P_r,T_r} - S^o_{P_r,T_r}(T - T_r) + \int_{T_r}^{T} C^o_{P_r} dT - T\int_{T_r}^{T} C^o_{P_r} d\ln T + \int_{P_r}^{P} V^o_T dP \tag{A3}$$

In that equation, $G^O_{P_r,T_r}$ and $S^O_{P_r,T_r}$ respectively represent the standard molal Gibbs energy and entropy at the reference temperature (T_r = 25 °C) and pressure (P_r = 1 bar). $C^o_{P_r}$ represents the standard molal heat capacity at P_r, and V^o_T denotes the standard molal volume at the temperature of interest. Values of $C^O_{P_r}$ as a function of temperature for solid and gaseous compounds can be calculated as (Helgeson et al. 1978, 1998; LaRowe and Dick 2012):

$$C^0_{P_r} = a + bT \tag{A4}$$

where a and b correspond to temperature-independent coefficients of the compounds of interest. Values of V^O_T for solid compounds were assumed to be equal to those of the standard molal volume at 25 °C and 1 bar $\left(V^o_{P_r,T_r}\right)$ in a range of temperature and pressure (Helgeson et al. 1998; LaRowe and Dick 2012). The value of V^O_T for H_2O(g) and its temperature and pressure dependences were calculated using the ideal gas law ($PV = RT$).

Table 3 presents the thermodynamic dataset used for the present calculations. All values were taken from the reports listed in the table legend. Exceptions are the values of $C^O_{P_r}$ at 25 °C, a, and b for DKP and H_2O(g), which were retrieved by simultaneous regression of experimental $C^o_{P_r}$ data as a function of temperature (Lebedev et al. 1981, 1982; Abate et al.

Table 3 Standard molal thermodynamic data at 25 °C and 1 bar and $C_p{}^o$ power function coefficients for crystalline compounds and H_2O(g)

Species	$\Delta_f G^o$[a]	$\Delta_f H^o$[a]	$S^o_{Pr,\ Tr}$[b]	$C_p{}^o$[b]	V^o[c]	a[b]	b[d]
Gly(s)	–368.40[e]	–528.10[f]	103.5[g]	99.24[g]	46.63[g]	14.90[g]	0.2829[g]
	(±1.1)	(±0.5)	(±2.1)	(±0.8)			
GlyGly(s)[g]	–489.10	–746.89	180.3	163.80	87.07	35.44	0.4304
	(±2.7)	(±2.1)	(±2.1)	(±0.8)			
DKP(s)	–244.86[e]	–443.50[h]	145.5[i]	134.37[j]	71.67[k]	20.57[j]	0.3817[j]
	(±8.5)	(±8.4)	(±0.3)	(± 0.06)[i]			
Gly_3(s)[g]	–608.80	–965.70	253.9	229.19	120.50	43.94	0.6212
	(±2.7)	(±2.1)	(±2.1)	(±0.8)			
H_2O(g)[l]	–228.58[e]	–241.83	188.8	33.61	24,790	32.52[m]	0.0040[m]
	(±0.04)	(±0.04)	(±0.01)	(±0.03)			

[a] kJ mol^{-1}

[b] J mol^{-1} K^{-1}

[c] cm^3 mol^{-1}

[d] J mol^{-1} K^{-2}

[e] calculated from $\Delta_f H^o$ and $S^o_{P_r,T_r}$ in the table together with values of $S^o_{P_r,T_r}$ of the elements (O_2(g), H_2(g), C(graphite), and N_2(g)) from Cox et al. (1989)

[f] Diaz et al. (1992)

[g] LaRowe and Dick (2012)

[h] Domalski (1972)

[i] Lebedev et al. (1981)

[j] from regression calculation (see the text)

[k] Barone and Puliti (1999)

[l] Cox et al. (1989)

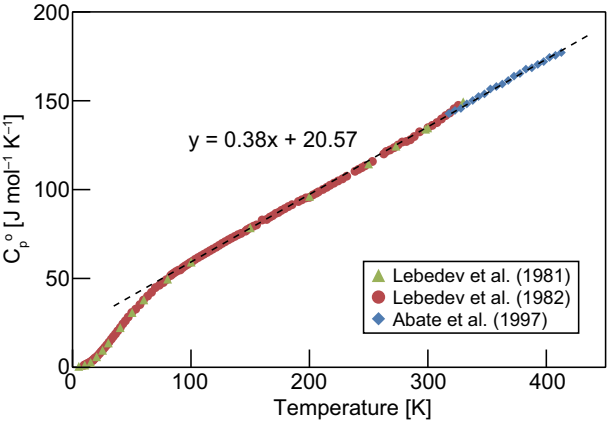

Fig. 8 Standard molal heat capacity ($C^o_{P_r}$) of DKP as a function of temperature at 1 bar. The regression line represents fit of Eq. (A4) to the experimental data reported in the literature (symbols) at >100 K

1997 for DKP and Cox et al. 1989 for $H_2O(g)$). Based on Eq. (A4), the intercept and slope of the regression line respectively correspond to *a* and *b*. The regression line was drawn for experimental $C^O_{P_r}$ data at >100 K for DKP and at 100–400 K for $H_2O(g)$ (e.g., Fig. 8). The value of $C^o_{P_r}$ at 25 °C for DKP was then calculated using the *a* and *b* values obtained from Eq. (A4).

References

Abate L, Palecz B, Giancola C, Gatta GD (1997) Heat capacities, and enthalpies and entropies of fusion of some uncharged small peptides (N-acetylamino acid amides and 2,5-diketopiperazines). J Chem Thermodynamics 29:359–368

Barone G, Puliti R (1999) Correlation between phase transition thermodynamics and crystal features of solid small peptides. J Thermal Ana Calorim 57:119–132

Basiuk VA (1992) Condensation of vaporous amino acids in the presence of silica. Formation of bi- and tricyclic amidines. Orig Life Evol Biosph 22:333–348

Basiuk VA, Gromovoy TY (1994) Free energies of adsorption of dipeptides and 2,5-piperazinediones on silica from neutral aqueous solutions as estimated from high-performance liquid-chromatographic retention data. Collect Czechoslov Chem Commun 59:1721–1728

Basiuk VA, Sainz-Rojas J (2001) Catalysis of peptide formation by inorganic oxides: high efficiency of alumina under mild conditions on the earth-life planets. Adv Space Res 27:225–230

Basiuk VA, Gromovoy TY, Golovaty VG, Glukhoy AM (1990–1991) mechanisms of amino acid polycondensation on silica and alumina surfaces. Orig Life Evol Biosph 20:483–498

Basiuk VA, Gromovoy TY, Glukhoy AM, Golovaty VG (1991) Chemical transformations of proteinogenic amino acids during their sublimation in the presence of silica. Orig Life Evol Biosph 21:129–144

Basiuk VA, Gromovoy TY, Khilchevskaya EG (1995) Adsorption of small biological molecules on silica from diluted aqueous solutions: quantitative characterization and implications to the Bernal's hypothesis. Orig Life Evol Biosph 25:375–393

Ben Shir I, Kababya S, Schmidt A (2012) Binding specificity of amino acids to amorphous silica surfaces: solid-state NMR of glycine on SBA-15. J Phys Chem C 116:9691–9702

Bujdak J, Rode BM (1997a) Glycine oligomerization on silica and alumina. React Kinet Catal Lett 62:281–286

Bujdak J, Rode BM (1997b) Silica, alumina, and clay-catalyzed alanine peptide bond formation. J Mol Evol 45: 457–466

Bujdak J, Rode BM (1999) Silica, alumina and clay catalyzed peptide bond formation: enhanced efficiency of alumina catalyst. Orig Life Evol Biosph 29:451–461

Bujdak J, Rode BM (2001) Activated alumina as an energy source for peptide bond formation: consequences for mineral-mediated prebiotic processes. Amino Acids 21:281–291

Bujdak J, Rode BM (2002) Preferential amino acid sequences in alumina-catalyzed peptide bond formation. J Inorg Biochem 90:1–7

Bujdak J, Rode BM (2003) Alumina catalyzed reactions of amino acids. J Therm Ana Calorim 73:797–805

Cleaves HJ, Scott AM, Hill FC, Leszczynski J, Sahai N, Hazen R (2012) Mineral–organic interfacial processes: potential roles in the origins of life. Chem Soc Rev 41:5502–5525
Costa D, Lomenech C, Meng M, Stievano L, Lambert JF (2007) Microsolvation of glycine by silanol ligands: a DFT study. J Mol Struct THEOCHEM 806:253–259
Cox JD, Wagman DD, Medvedev VA (1989) COVATA Key Values for Thermodynamics. Hemisphere Publishing Corp, New York
Deiana C, Sakhno Y, Fabbiani M, Pazzi M, Vincenti M, Martra G (2013) Direct synthesis of amides from carboxylic acids and amines by using heterogeneous catalysts: evidence of surface carboxylates as activated electrophilic species. ChemCatChem 5:2832–2834
Diaz EL, Domalskia ES, Colbertc JC (1992) Enthalpies of combustion of glycylglycine and DL-alanyl-DL-alanine. J Chem Thermodyn 24:1311–1318
Domalski ES (1972) Selected values of heats of combustion and heats of formation of organic compounds containing the elements C, H, N, O, P, and S. J Phys Chem Ref Data 1:221–277
Garcia AR, de Barros RB, Fidalgo A, Ilharco LM (2007) Interactions of L-alanine with alumina as studied by vibrational spectroscopy. Langmuir 23:10164–10175
Georgelin T, Jaber M, Bazzi H, Labmert JF (2013) Formation of activated biomolecules by condensation on mineral surfaces – a comparison of peptide bond formation and phosphate condensation. Orig Life Evol Biosph 43:429–443
Glavin DP, Callahan MP, Dworkin JP, Elsila JE (2011) The effects of parent body processes on amino acids in carbonaceous chondrites. Meteorit Planet Sci 45:1948–1972
Gromovoy T, Basiuk VA, Chuiko AA (1991) Growth of peptide chains on silica in absence of amino acid access from without. Orig Life Evol Biosph 21:119–128
Hazen RM, Papineau D, Bleeker W, Downs RT, Ferry JM, McCoy TJ, Sverjensky DA, Yang H (2008) Am Mineral 93:1693–1720
Helgeson HC, Delany JM, Nesbitt HW, Bird DK (1978) Summary and critique of the thermodynamic properties of rock-forming minerals. Am J Sci 278:1–229
Helgeson HC, Owens CE, Knox AM, Richard L (1998) Calculation of the standard molal thermodynamic properties of crystalline, liquid, and gas organic molecules at high temperatures and pressures. Geochim Cosmochim Acta 62:985–1081
Jaber M, Spadavecchia J, Bazzi H, Georgelin T, Costa-Torro F, Lambert JF (2013) Non-biological selectivity in amino acids polymerization on TiO_2 nanoparticles. Amino Acids 45:403–406
Jonsson PG, Kvick A (1972) Precision neutron diffraction structure determination of protein and nucleic acid components. III. The crystal and molecular structure of the amino acid α-glycine. Acta Cryst B28:1827–1833
Kelber JA (2007) Alumina surfaces and interfaces under non-ultrahigh vacuum conditions. Surf Sci Rep 62:271–303
Kitadai N (2014) Thermodynamic prediction of glycine polymerization as a function of temperature and pH consistent with experimentally obtained results. J Mol Evol 78:171–187
Kitadai N, Yokoyama T, Nakashima S (2011) Hydration –dehydration interactions between glycine and anhydrous salts: implications for a chemical evolution of life. Geochim Cosmochim Acta 75:6285–6299
Lambert JF (2008) Adsorption and polymerization of amino acids on mineral surfaces: a review. Orig Life Evol Biosph 38:211–242
Lambert JF (2009) The fate of amino acids adsorbed onto mineral matter. Planet Space Sci 57:460–467
Lambert JF, Jaber M, Georgelin T, Stievano L (2013) A comparative study of the catalysis of peptide bond formation by oxide surfaces. Phys Chem Chem Phys 15:13371–13380
LaRowe DE, Dick JM (2012) Calculation of the standard molal thermodynamic properties of crystalline peptides. Geochim Cosmochim Acta 80:70–91
Lebedev BV, Kulagina TG, Kiparisova EG (1981) Thermodynamics of 2,5-piperadinedione in the range of 0–330 K. Zhuranal Obshchei Khimii 51:199–203
Lebedev BV, Kulagina TG, Kiparisova EG (1982) Thermodynamics of *dl*-lactide, ethylene oxalate, and 2,5-dioxopiperazine in the range 0–330 K. Russ J Phys Chem 56:1641–1643
Lerotholi TJ, Kroger EA, Knight MJ, Unterberger W, Hogan K, Jackson DC, Lamont CLA, Woodruff DP (2009) Adsorption structure of glycine on TiO2(110): a photoelectron diffraction determination. Surf Sci 603:2305–2311
Leyton P, Zarate RA, Fuentes S, Paipa C, Gomez-Jeria JS, Leyton Y (2011) Influence of aluminum oxide on the prebiotic thermal synthesis of Gly-Gly-$(Gly\text{-}Gly)_n$ polymer. Biosystems 104:118–126
Leyton P, Saladino R, Crestini C, Campos-Vallette M, Paipa C, Berrios A, Fuentes S, Zarate RA (2012) Influence of TiO_2 on prebiotic thermal synthesis of the Gly-Gln polymer. Amino Acids 42:2079–2088
Lomenech C, Bery G, Costa D, Stievano L, Lambert JF (2005) Theoretical and experimental study of the adsorption of neutral glycine on silica from the gas phase. ChemPhysChem 6:1061–1070

Martra G, Deiana C, Sakhno Y, Barberis I, Fabbiani M, Pazzi M, Vincenti M (2014) The formation and self-assembly of long prebiotic oligomers produced by the condensation of unactivated amino acids on oxide surfaces. Angew Chem Int Ed 53:4671–4674

Matrajt G, Blanot D (2004) Properties of synthetic ferrihydrite as an amino acid adsorbent and a promoter of peptide bond formation. Amino Acids 26:153–158

Meng M, Stievano L, Lambert JF (2004) Adsorption and thermal condensation mechanisms of amino acids on oxide supports. 1. Glycine on silica. Langmuir 20:914–923

Monti S, van Duin ACT, Kim SY, Barone V (2012) Exploration of the comformational and reactive dynamics of glycine and diglycine on TiO_2: computational investigations in the gas phase and in solution. J Phys Chem C 116:5141–5150

Ogawa H, Fujigaki T, Chihara T (1999) Selective formation of glycylglycine by dehydration of glycine adsorbed onto silica gel. J Phys Org Chem 12:354–356

Pokrovsky OS, Schott J (2000) Forsterite surface composition in aqueous solutions: a combined potentiometric, electrokinetic, and spectroscopic approach. Geochim Cosmochim Acta 64:3299–3312

Qiu T, Barteau MA (2006) STM study of glycine on TiO_2(110) single crystal surfaces. J Colloid Interface Sci 303:229–235

Rimola A, Costa D, Sodupe M, Lambert JF, Ugliengo P (2013) Silica surface features and their role in the adsorption of biomolecules: computational modeling and experiments. Chem Rev 113:4216–4313

Rode BM (1999) Peptides and the origin of life. Peptides 20:773–786

Sakata K, Kitadai N, Yokoyama T (2010) Effects of pH and temperature on dimerization rate of glycine: evaluation of favorable environmental conditions for chemical evolution of life. Geochim Cosmochim Acta 74:6841–6851

Schoonen M, Smirnov A, Cohn C (2004) A perspective on the roe of minerals in prebiotic synthesis. Ambio 33: 539–551

Shanker U, Bhushan B, Bhattacharjee G, Kamaluddin (2012) Oligomerization of glycine and alanine catalyzed by iron oxides: implications for prebiotic chemistry. Orig Life Evol Biosph 42:31–45

Stievano L, Piao LY, Lopes I, Meng M, Costa D, Lambert JF (2007) Glycine and lysine adsorption and reactivity on the surface of amorphous silica. Eur J Mineral 19:321–331

Stueken EE, Anderson RE, Bowman JS, Brazelton WJ, Colangelo-Lillis J, Goldman AD, Som SM, Baross JA (2013) Did life originate from a global chemical reactor? Geobiology 11:101–126

Sverjensky DA (2005) Prediction of surface charge on oxides in salt solutions: revisions for 1:1 (M^+L^-) electrolytes. Geochim Cosmochim Acta 69:225–257

Szieberth D, Ferrari AM, Dong X (2010) Adsorption of glycine on the anatase (101) surface: an *ab initio* study. Phys Chem Chem Phys 12:11033–11040

Thomas AG, Syres KL (2012) Adsorption of organic molecules on rutile TiO_2 and anatase TiO_2 single crystal surfaces. Chem Soc Rev 41:4207–4217

Tonner R (2010) Adsorption of proline and glycine on the TiO_2(110) surface: a density functional theory study. ChemPhysChem 11:1053–1061

Tzvetkov G, Koller G, Zubavichus Y, Fuchs O, Casu MB, Heske C, Umbach E, Grunze M, Ramsey MG, Netzer FP (2004) Bonding and structure of glycine on ordered Al_2O_3 film surfaces. Langmuir 20:10551–10559

Wilson JN, Dowler RM, Idriss H (2011) Adsorption and reaction of glycine on the rutile TiO_2(011) single crystal surface. Surf Sci 605:206–213

Wu J, Zhang ZS, Yu XW, Pan HH, Jiang WG, Xu XR, Tang RK (2011) Mechanism of promoted dipeptide formation on hydroxyapatite crystal surfaces. Chin Sci Bull 56:633–639

Zaia DAM, Zaia CTBV, De Santana H (2008) Which amino acids should be used in prebiotic chemistry studies? Orig Life Evol Biosph 38:469–488